Article:

Huang, L., Zhu, Z.Q. orcid.org/0000-0001-7175-3307, Feng, J. et al. (3 more authors) (2019) Analysis of Stator/Rotor Pole Combinations in Variable Flux Reluctance Machines Using Magnetic Gearing Effect. IEEE Transactions on Industry Applications, 55 (2). pp. 1495-1504. ISSN 0093-9994

https://doi.org/10.1109/TIA.2018.2883608

Analysis of Stator/Rotor Pole Combinations in Variable Flux Reluctance Machines Using Magnetic Gearing Effect

L.R. Huang, Z.Q. Zhu, Fellow, IEEE
Department of Electronic and Electrical Engineering
The University of Sheffield, Sheffield S1 3JD, UK
lhuang18@sheffield.ac.uk, z.q.zhu@sheffield. ac.uk

J.H. Feng, S.Y. Guo, J.X. Shi, W.Q. Chu
CRRC Zhuzhou Institute Co. Ltd
Shidai Road, Shifeng District, Zhuzhou, Hunan, China
fengjh@csrzic.com, guosy@csrzic.com,
shijx2@csrzic.com, wenqiang_chu@dynexsemi.com

Abstract—The torque production of variable flux reluctance machines (VFRMs) is explained by the "magnetic gearing effect" in recent research. Based on this theory, this paper concludes the general principles for feasible stator/rotor pole selection and corresponding winding configuration for VFRMs. The influence of stator/rotor pole combination on torque performance is comprehensively investigated not only in terms of average torque and torque ripple, but also in terms of each single torque component. It is found that the synchronous torque is proportional to the fundamental rotor radial permeance component and has the dominant contribution in average torque for all the VFRMs. The stator slot number and rotor pole number should be close to each other to achieve the highest output torque. Meanwhile, the 6-stator-slot/(6i±2)-rotor-pole (6s/(6i±2)r) and their multiples are large torque ripple origins for VFRMs due to the large reluctance torque ripple. Also, it is proved that a lower stator slot number is preferable choice to obtain higher torque/copper loss ratio, whereas a higher stator slot number is more suitable for large machine scale scenario. Finally, the analyses and conclusions are verified by finite element analysis (FEA) on the 6-, 12-, 18- and 24-stator-slot VFRMs and by experimental tests on a 6s/7r and 6s/8r VFRMs.

Keywords— Magnetic gearing effect, stator/rotor pole combination, variable flux reluctance machine

NOMENCLATURE

A_s	Total stator slot area
F	Magnetomotive force (MMF)
F_a, F_f	MMFs of armature and field currents
F_s	Modulated MMF
F_{s1}, F_{s2}	General expressions of modulated MMFs
F_{sa}, F_{sf}	Modulated MMFs of armature and field currents
g_0	Airgap length
I_a, I_f	RMS currents of armature and field windings
k_T	Torque coefficient
L_{end}	End length of windings
L_{stk}	Machine stack length
N_c	Turns per coil
N_p	Number of iron modulators in a magnetic gear
N_s, N_r	Numbers of stator/rotor slots
p	Pole pair number
P_a, P_f	Spatial harmonic orders of modulated MMFs for armature and field currents
P_{cu}	Total copper loss of VFRM
P_{cua}, P_{cuf}	Copper losses of armature and field currents
P_o, P_i	PM pole-pair numbers of outer and inner rotors of a magnetic gear
R_{si}	Radius of stator inner surface
T_e	Electromagnetic torque
T_{e_avg}	Average value of electromagnetic torque
T_{ep}	Electromagnetic torque component
T_s, T_r, T_c	Synchronous/reluctance/cogging torques
T_{s_avg}, T_{r_avg}, T_{c_avg}	Average value of synchronous/ reluctance/ cogging torques
T_{s_rip}, T_{r_rip}, T_{c_rip}	Synchronous/reluctance/cogging torque ripples
θ	Mechanical angle
θ_{ro}	Rotor initial position in mechanical degree
Λ_{r0}, Λ_{rk}	Magnitudes of DC and k-th rotor radial permenace harmonics
Λ_s, Λ_r	Stator and rotor permeance functions obtained by single-side saliency model
μ_0	Vacuum permeability
ρ_{cu}	Resistivity of copper
Ω_a	Rotating speed of P_a-th armature modulated MMF harmonics
Ω_f	Rotating speed of P_f-th field modulated MMF harmonics
Ω_N, Ω_o, Ω_i	Rotating speed of outer rotor, inner rotor and iron pieces of a magnetic gear
Ω_r	Rotor mechanical rotating speed

I. INTRODUCTION

Variable flux reluctance machines (VFRMs) are one kind of magnetless machines developed in recent years [1], [2]. Fig. 1 shows the configurations of five typical VFRMs, i.e., 6-stator-pole/2-rotor-pole (6s/2r), 6s/4r, 6s/5r, 6s/7r and 6s/8r VFRMs. They have doubly salient structures, which are similar to the switched reluctance machines (SRMs), and two sets of stator-located concentrated windings, i.e., AC armature and DC field windings. Due to the common structure features, VFRMs have low torque density and power factor issues as SRMs. In addition, the introduction of field current increases the complexity of the control system, although it also provides an additional flexible control parameter. Nevertheless, VFRMs have many advantages, e.g., significantly reduced acoustic noise [3], more flexible stator/rotor pole combinations [4], [5], feasible application of commercial inverter. Moreover, the robust structures and the absence of permanent magnet enable VFRMs to be applied in a harsh operation environment, high temperature and aerospace actuators for example.

For machine design, proper stator/rotor pole combination is known to be an important criterion to enhance the performance. By way of examples, in [6]-[11], the influence of stator/rotor pole combinations on electromagnetic performance is investigated for various machines, e.g., SRMs [6], [7], permanent magnet (PM) synchronous machines [8], [9], flux switching PM machines [10], synchronous reluctance machines [11]. As for VFRMs, the electromagnetic performance of 6s/(4, 5, 7, 8)r and 12s/(8, 10, 11, 13, 14)r VFRMs are comparatively analyzed in [5] and [12], respectively. Then, [13] establishes the relationship between stator/rotor pole combination and armature winding pole pairs. However, in these work, the performance evaluation relies on finite element analysis (FEA), which is complicated in modelling and performance estimation. As a further step, [14] and this paper investigates the influence of stator/rotor pole combination on the torque production from the perspective of magnetic gearing effect [15][16]. Specifically, the difference between various stator/rotor pole combinations will reflect on their spatial MMF and permeance harmonics, which are eventually linked to the output torque by the magnetic gearing effect theory. With this method, the average torque and torque ripple productions due to synchronous, reluctance and cogging torque components can be separately analyzed. More importantly, the torque characteristics of VFRMs can be easily predicted with some simple figures which are directly deduced from the rotor pole number and winding configurations.

The paper is organized as follows: In Section II, the magnetic gearing effect in the torque production of VFRMs is revealed based on an analytical model. In Section III, the principles of feasible stator/rotor pole selection and corresponding winding configuration are illustrated. In Section IV, the torque characteristics of 6-stator-slot VFRMs are investigated in detail and then extended to 12-, 18- and 24-stator-slot VFRMs. In Section V, the revealed torque characteristics are validated by the FEA results on (6, 12, 18, 24)s/(2,4,5…20)r VFRMs and the test of a 6s/7r VFRM prototype.

II. Magnetic Gearing Effect in VFRM

A. Torque expression of VFRMs

Based on the Lorentz force law, the instantaneous torque equation of VFRM can be expressed as (1). The detailed derivation procedure and validation is illustrated in [16].

$$T_e(t) = -R_{si}L_{stk}\int_0^{2\pi}\left(F_{sa}+F_{sf}\right)\Lambda_r d\left(F_{sa}+F_{sf}\right) \tag{1}$$

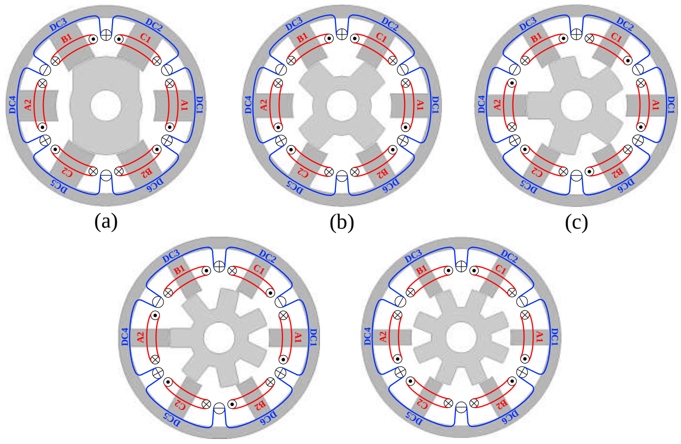

Fig. 1. Configurations of the VFRMs with different stator/rotor pole combinations. (a) 6s/2r. (b) 6s/4r. (c) 6s/5r. (d) 6s/7r. (e) 6s/8r.

where R_{si} is the radius of stator inner surface; L_{stk} is the machine stack length; θ is the mechanical angle in the stator reference frame; Λ_r is the rotor radial permeance function obtained by salient rotor and slotless stator model; and F_{sa} and F_{sf} are the "modulated MMFs" of armature and field windings, which are defined by:

$$\begin{cases} F_{sa}(\theta,t) = F_a(\theta,t)g_0\Lambda_s(\theta)/\mu_0 \\ F_{sf}(\theta,t) = F_f(\theta,t)g_0\Lambda_s(\theta)/\mu_0 \end{cases} \tag{2}$$

where g_0 is the airgap length; μ_0 is the vacuum permeability; Λ_s is the stator radial permeance function obtained by the smooth rotor and slotted stator model; F_a (θ, t) and F_f (θ, t) are the MMFs of armature and field currents, respectively.

As proved in [16], the modulated MMFs of armature and field currents are identical to their corresponding MMFs in terms of harmonic order and corresponding rotating speed, albeit with modified harmonic magnitude due to the modulation effect of stator slot effect. In this case, the spatial harmonic content of modulated MMF can be easily deduced from winding theory [17].

Then, by substituting (2) into (1), the torque equation can be divided into three components: synchronous torque T_s, reluctance torque T_r and cogging torque T_c, i.e. [16]

$$\begin{aligned} T_e(t) = &-R_{si}L_{stk}\int_0^{2\pi}\frac{\Lambda_r(\theta,t)}{2}\frac{dF_{sa}^2(\theta,t)}{d\theta} - && \text{① } T_r \\ &R_{si}L_{stk}\int_0^{2\pi}\frac{\Lambda_r(\theta,t)}{2}\frac{dF_{sf}^2(\theta,t)}{d\theta} - && \text{② } T_c \\ &R_{si}L_{stk}\int_0^{2\pi}\Lambda_r(\theta,t)\frac{d\left[F_{sa}(\theta,t)F_{sf}(\theta,t)\right]}{d\theta} && \text{③ } T_s \end{aligned} \tag{3}$$

where F_{sa} (θ, t) and F_{sf} (θ, t) are the modulated MMFs of armature and field currents, respectively.

It can be found that component-1 and component-2 are generated by either armature or field modulated MMF only, while component-3 is generated by the interaction of armature and field modulated MMFs. According to the common torque definitions in electrical machines, torque components-1, 2 and 3 represent the reluctance torque T_r, cogging torque T_c and synchronous torque T_s, respectively.

B. Magnetic gearing effect in VFRM torque production

Further, from (3), it can be found that all these three torque components are generated by two interactive modulated MMFs and can be generally summarized as:

$$\begin{cases} T_{ep}(t) = -a\int_0^{2\pi}\Lambda_r(\theta,t)\dfrac{d\left[F_{s1}(\theta,t)F_{s2}(\theta,t)\right]}{d\theta} \\ a = \begin{cases} R_{si}L_{stk}/2 & \text{for } T_r \text{ or } T_c \\ R_{si}L_{stk} & \text{for } T_s \end{cases} \end{cases} \tag{4}$$

where F_{s1} and F_{s2} are modulated MMFs and could be either F_{sa} or F_{sf}; T_{ep} could be either T_s, T_r or T_c depending on the interactive F_{s1} and F_{s2}. For instance, if F_{s1} and F_{s2} are both F_{sa}, T_{ep} then represents reluctance torque T_r according to (3).

Letting the general Fourier series expressions of two interactive modulated MMFs and rotor radial permeance functions to be:

$$\begin{cases} F_{s1}(\theta,t) = \sum\limits_{m=1}^{\infty} f_m\cos\left(P_m\theta - \Omega_m t - \theta_m\right) \\ F_{s2}(\theta,t) = \sum\limits_{n=1}^{\infty} f_n\cos\left(P_n\theta - \Omega_n t - \theta_n\right) \end{cases} \tag{5}$$

$$\Lambda_r(\theta,t) = \Lambda_{r0} + \sum_{k=1}^{\infty}\Lambda_{rk}\cos\left[kN_r\left(\theta - \Omega_r t - \theta_{r0}\right)\right] \tag{6}$$

where (f_m, f_n), (Ω_m, Ω_n) and (θ_m, θ_n) are the magnitudes, rotating speeds and advanced angles of the (P_m, P_n) -th harmonics of modulated MMFs (F_{s1}, F_{s2}). Λ_{r0} and Λ_{rk} are the magnitudes of the dc and the k-th rotor permeance harmonics, respectively; N_r is the number of rotor teeth; Ω_r is the rotor mechanical rotating speed; and θ_{r0} is the rotor initial position.

Then, by substituting (5) and (6) into (4), the average torque and torque ripple can be separated using harmonic analysis [16], i.e.

$$\begin{cases} T_{ep\_avg} = \sum\limits_{k=1}^{\infty}\sum\limits_{m=1}^{\infty}\sum\limits_{n=1}^{\infty}\Delta T(k,m,n) = \sum\limits_{k=1}^{\infty}\sum\limits_{m=1}^{\infty}\sum\limits_{n=1}^{\infty}\dfrac{af_m f_n kN_r\Lambda_{rk}\pi}{2}\sin(\delta) \\ \delta = \begin{cases} kN_r\theta_{r0} - \theta_1, & \begin{cases} kN_r = P_1 \\ kN_r\Omega_r = \Omega_1 \end{cases} \\ kN_r\theta_{r0} - \mathrm{sgn}(P_2)\theta_2, & \begin{cases} kN_r = |P_2| \\ kN_r\Omega_r = \mathrm{sgn}(P_2)\Omega_2 \end{cases} \end{cases} \end{cases} \tag{7}$$

$$\begin{cases} T_{ep\_rip}(t) = \sum\limits_{k=1}^{\infty}\sum\limits_{m=1}^{\infty}\sum\limits_{n=1}^{\infty}\Delta T(k,m,n) = \sum\limits_{k=1}^{\infty}\sum\limits_{m=1}^{\infty}\sum\limits_{n=1}^{\infty}\dfrac{af_m f_n kN_r\Lambda_{rk}\pi}{2}\sin(\psi) \\ \psi = \begin{cases} (kN_r\Omega_r - \Omega_1)t + kN_r\theta_{r0} - \theta_1, & \begin{cases} kN_r = P_1 \\ kN_r\Omega_r \neq \Omega_1 \end{cases} \\ \begin{matrix} \left[kN_r\Omega_r - \mathrm{sgn}(P_2)\Omega_2\right]t + \\ kN_r\theta_{r0} - \mathrm{sgn}(P_2)\theta_2 \end{matrix}, & \begin{cases} kN_r = |P_2| \\ kN_r\Omega_r \neq \mathrm{sgn}(P_2)\Omega_2 \end{cases} \end{cases} \end{cases} \tag{8}$$

where "sgn" is the sign function; T_{ep_avg} and T_{ep_rip} are the average torque and torque ripple of electromagnetic torque; $\Delta T(k, m, n)$ is the elementary torque component generated by k-the rotor permeance, m-th F_{s1} and n-th F_{s2} components; and

$$\begin{cases} P_1 = P_m + P_n,\ \Omega_1 = \Omega_m + \Omega_n,\ \theta_1 = \theta_m + \theta_n \\ P_2 = P_m - P_n,\ \Omega_2 = \Omega_m - \Omega_n,\ \theta_2 = \theta_m - \theta_n \end{cases} \tag{9}$$

From (7)-(9), the operation principle of VFRMs can be revealed, as shown in Fig. 2. Basically, two specific field com-

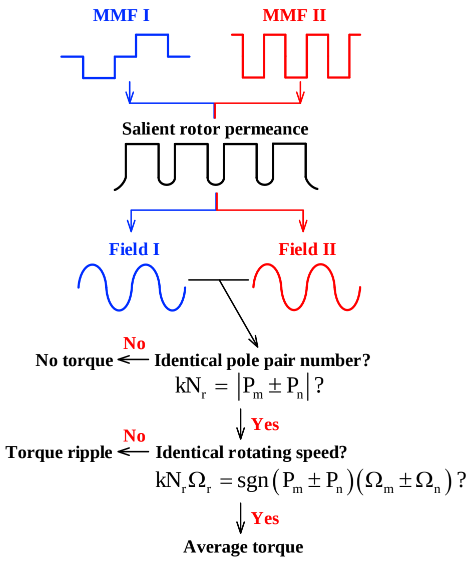

Fig. 2. Operation principle of VFRMs.

ponents are generated by the P_m-th component of MMF F_{s1}, P_n-th component of MMF F_{s2}, and the modulation effect of kN_r-th component of rotor permeance. Their interaction can lead to average torque only when conditions (10) and (11) are satisfied simultaneously.

$$kN_r = |P_m \pm P_n| \tag{10}$$

$$kN_r\Omega_r = \mathrm{sgn}(P_m \pm P_n)(\Omega_m \pm \Omega_n) \tag{11}$$

The magnitude of torque is governed by:

$$T_{avg}(kN_r, P_m, P_n) \propto kN_r\Lambda_{rk} f_m f_n \tag{12}$$

However, if only condition (10) is satisfied, the torque ripple rather than average torque will be resulted. The number of fluctuation over one electrical period N_{ripple} is:

$$N_{ripple} = \left| k - \frac{\mathrm{sgn}(P_m \pm P_n)(\Omega_m \pm \Omega_n)}{N_r\Omega_r} \right| \tag{13}$$

Since condition (10) is essential for both average torque and torque ripple productions, a specific combination of P_m-th component of MMF F_{s1}, P_n-th component of MMF F_{s2}, and kN_r-th component of rotor permeance, which satisfies (10) is defined as a "magnetic gear pair" in following investigation.

It can be found that the condition (10) is similar to that of magnetic gears [18]:

$$N_p = |P_o + hP_i|,\ \ h = \pm 1 \tag{14}$$

where P_o and P_i are the PM pole-pair numbers of outer and inner rotor; N_p is the number of iron pieces in magnetic gear.

Further, (12) also agrees with the synchronous rotating speed principle in magnetic gears for active torque generation, i.e.

$$N_p\Omega_N = P_o\Omega_o + hP_i\Omega_i,\ \ h = \pm 1 \tag{15}$$

where Ω_o, Ω_i and Ω_N are the rotating speed of outer rotor, inner rotor and iron pieces, respectively.

Overall, the interactive modulated MMF harmonics play the role of the outer and inner PMs of a magnetic gear, whereas the rotor permeance harmonics is equivalent to the iron pieces in a magnetic gear. This is the so-called “magnetic gearing effect” [15][16] or “airgap field modulation effect” [19]. However, different from the single working harmonic in actual magnetic gear, VFRM is usually working with multi-harmonics, which makes it more complicated and interesting to investigate the influence of different stator/rotor pole.

III. Principle of Stator/Rotor Pole Selection

One feasible stator/rotor pole combination means that its average torque is nonzero. In this case, conditions (10) and (11) should be satisfied simultaneously. In this section, the 6-stator-slot VFRMs are investigated as examples first. Then, the revealed principle is extended to all the VFRMs.

Due to the double layer and concentrated winding type, the armature winding of 6-stator-slot VFRMs can be configured into 6-stator-slot/2-poles (6s/2p) or 6s/4p, whereas the field winding has only one configuration with 6 poles, as shown in Fig. 3. Based on the conventional winding theory of AC machine, the armature coils can then be configured into three phases according to their back-EMF phasor diagrams, as shown in Fig. 4. Eventually, the spatial harmonic contents of modulated MMFs can be deduced, as shown in Table I.

According to [16], the average torque of VFRM is mainly generated by the interaction between AC and DC currents, which is denoted by ‘synchronous torque’ in (4). To generate nonzero synchronous torque, conditions (10) and (11) should be satisfied.

By substituting the harmonic order and rotating speed of modulated MMFs into (10) and (11), it is found that the condition (11) is satisfied only when k=1. In this case, the feasible rotor pole number selection for a specific armature and field winding configuration is derived from (16):

$$N_r = |P_a \pm P_f| \tag{16}$$

where P_a and P_f are the spatial harmonic orders of modulated MMFs for armature and field currents

For example, the feasible rotor pole number for armature winding I can be selected as:

$$N_r = |P_a \pm P_f| = |(6n\pm1)\pm(6m+3)| = |6r\pm2| \quad (m,\ n,\ r = 0,1,2...) \tag{17}$$

Similarly, the feasible rotor pole number for armature winding II can also be obtained:

$$N_r = |P_a \pm P_f| = |(6n\pm2)\pm(6m+3)| = |6r\pm1| \quad (m,\ n,\ r = 0,1,2...) \tag{18}$$

It can be seen that for armature winding I, all the even numbers except multiple of 3 can be chosen for rotor pole number, i.e., 2, 4, 8, 10…. In contrast, all the odd numbers except multiple of 3 are feasible for armature winding II, i.e., 5, 7, 11, 13….

By applying this principle to VFRMs with 6-, 12-, 18-, 24-stator-slot, all the feasible stator/rotor pole combination and corresponding armature winding configurations are listed in Table II. It can be seen that some VFRMs are with odd rotor pole number. Due to the asymmetric electromagnetic structure, there will be unbalanced magnetic force in these combinations. Nevertheless, this can be eliminated by simply doubling both stator slot and rotor pole numbers.

TABLE I
Harmonic Contents of Modulated MMFs

Winding configuration	Harmonic order	Rotating speed
Armature I (6s/2p)	6n+1	$N_r\Omega_r$
	6n-1	$-N_r\Omega_r$
Armature II (6s/4p)	6n+2	$N_r\Omega_r$
	6n-2	$-N_r\Omega_r$
Field winding	6m+3	0

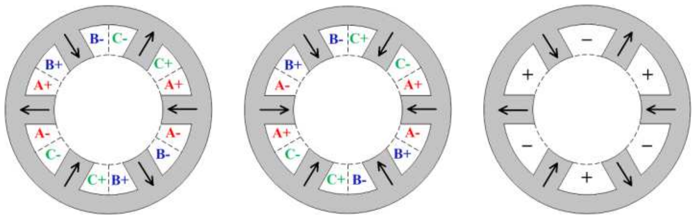

(a) (b) (c)

Fig. 3. Winding configurations for armature and field windings in VFRMs. (a) Armature winding I (6s/2p). (b) Armature winding II (6s/4p). (c) Field winding.

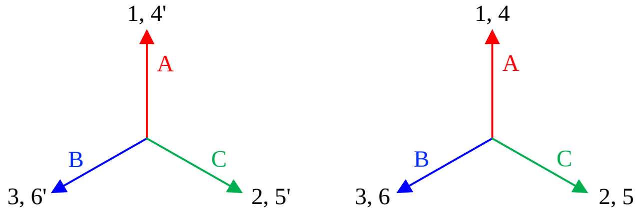

(a) (b)

Fig. 4. Armature coil back-EMF phasors for 6s/2p and 6s/4p configurations. (a) Armature winding I (6s/2p). (b) Armature winding II (6s/4p).

IV. Torque Characteristics of VFRMs with Different Stator/Rotor Pole Combinations

In order to analyze the torque characteristics of VFRM with different stator/rotor pole combinations, the specific magnetic gear pairs which contribute to the average value and ripple of synchronous, reluctance and cogging torque components can be identified by using conditions (10) and (11). In this paper, the 6s/(2, 4, 5, 7, 8)r VFRMs are analyzed in detail as examples first. The revealed characteristics are then extended to other

TABLE II
Feasible Stator/Rotor Pole Combinations for 6-, 12-, 18- and 24-stator-slot VFRMs

Stator slots	6		12				18					
Field winding poles	6		12				18					
Field MMF harmonic	6m+3		12m+6				18m+9					
Armature winding poles	2	4	2	4	8	10	2	4	8	10	14	16
Armature MMF harmonic	6n±1	6n±2	12n±1	12n±2	12n±4	12n±5	18n±1	18n±2	18n±4	18n±5	18n±7	18n±8
Feasible rotor pole no.	|6i±2|	|6i±1|	|12i±5|	|12i±4|	|12i±2|	|12i±1|	|18i±8|	|18i±7|	|18i±5|	|18i±4|	|18i±2|	|18i±1|
Specific rotor pole no.	2,4,8	5,7,11	5,7,17	4,8,16	2,10,14	11,13,23	8,10,26	7,11,25	5,13,23	4,14,22	2,16,20	17,19,35

Stator slots	24							
Field winding poles	24							
Field MMF harmonic	24m+12							
Armature winding poles	2	4	8	10	14	16	20	22
Armature MMF harmonic	24n±1	24n±2	24n±4	24n±5	24n±7	24n±8	24n±10	24n±11
Feasible rotor pole no.	|24i±11|	|24i±10|	|24i±8|	|24i±7|	|24i±5|	|24i±4|	|24i±2|	|24i±1|
Specific rotor pole no.	11,13,35	10,14,34	8,16,32	7,17,31	5,19,29	4,20,28	2,22,26	23,25,47

m, n, i=0,1,2,… ▭-Large torque ripple selections

VFRMs. Moreover, as can be seen from (12), the magnitude of the torque production for each magnetic gear pair is proportional to its corresponding modulated MMF harmonics. Hence, only the dominant harmonics of modulated MMF (1^{st}, 5^{th}, 7^{th} and 11^{th} harmonics for armature winding I, 2^{nd}, 4^{th}, 8^{th} and 10^{th} harmonics for armature winding II, 3^{rd} and 9^{th} harmonics for field winding) are taken into account. The higher order harmonics are relatively small and only contribute to negligible torque components. They are therefore neglected.

A. Average torque

Table III shows the dominant magnetic gear pairs which contribute to the average torque in 6s/(2, 4, 5, 7, 8)r VFRMs. For clarity, the components which have significantly large magnitudes are marked by grey color. The modulated MMFs of armature and field windings F_{sa} and F_{sf} are simplified into A and F, respectively. The average values of synchronous, reluctance and cogging torque are represented by T_{s_avg}, T_{r_avg}, T_{c_avg}, respectively.

Several characteristics can be revealed:

(1) The average value of cogging torque is always 0.

(2) The average values of synchronous torque and reluctance torque are proportional to the magnitudes of the 1^{st} and 2^{nd} rotor radial permeance components, respectively.

(3) The synchronous torque is the dominant part for average torque production since the 1^{st} harmonic is usually the largest among all the harmonics in rotor radial permeance. In this case, the advanced current angle is close to 0 deg. and the average torque can be assumed to contain synchronous torque only. Its average torque can then be concisely summarized as:

$$T_{e\_avg} \approx T_{s\_avg} = k_T N_r \Lambda_{r1} I_a I_f \tag{19}$$

where k_T is the torque coefficient determined by winding configurations and machine structural parameters; Λ_{r1} is the magnitude of 1^{st} rotor radial permeance harmonic; I_a and I_f are the RMS currents of armature and field windings, respectively.

Further, by applying the same method, it can be found that all the aforementioned conclusions also fit VFRMs with other stator/rotor pole combinations listed in Table II. Therefore, the torque production of VFRMs is from the synchronous torque component rather than the reluctance torque component.

B. Torque ripple

Table IV shows the dominant magnetic gear pairs which contribute to the torque ripple in 6s/(2, 4, 5, 7, 8)r VFRMs. For clarity, the components which have significantly large magnitudes are marked by grey color. The ripples of synchronous, reluctance and cogging torque are represented by T_{s_rip}, T_{r_rip}, T_{c_rip}, respectively. It can be found that:

(a) All three torque components will contribute to the torque ripple. The fluctuation times of ripple over one electrical period is LCM(N_s, N_r)/N_r (LCM is least common multiple).

(b) For 6s/|6i±2|r (i=0,1,2,…) VFRMs, the reluctance torque component contributes to the largest torque ripple since it is proportional to the 1^{st} rotor permeance harmonic.

TABLE III
MAGNETIC GEAR PAIRS OF AVERAGE TORQUE FOR 6S/(2, 4, 5, 7, 8)R VFRMS

VFRM	Average torque	Permeance	kN_r	Source-harmonic order	
		Λ_{rk}		P_m	P_n
6s/2r	$^{\Delta}T_{s\_avg}$	Λ_{r1}	2	*A-1	†F-3
				A-5	F-3
				A-7	F-9
	T_{r_avg}	Λ_{r2}	4	A-1	A-5
	T_{c_avg}	-	-	-	-
6s/4r	T_{s_avg}	Λ_{r1}	4	A-1	F-3
				A-5	F-9
				A-7	F-3
	T_{r_avg}	Λ_{r2}	8	A-1	A-7
	T_{c_avg}	-	-	-	-
6s/5r	T_{s_avg}	Λ_{r1}	5	A-2	F-3
				A-4	F-9
				A-8	F-3
	T_{r_avg}	Λ_{r2}	10	A-2	A-8
	T_{c_avg}	-	-	-	-
6s/7r	T_{s_avg}	Λ_{r1}	7	A-2	F-9
				A-4	F-3
				A-10	F-3
	T_{r_avg}	Λ_{r2}	14	A-4	A-10
	T_{c_avg}	-	-	-	-
6s/8r	T_{s_avg}	Λ_{r1}	8	A-1	F-9
				A-5	F-3
				A-11	F-3
	T_{r_avg}	Λ_{r2}	16	A-5	A-11
	T_{c_avg}	-	-	-	-

$^{\Delta}T_{s\_avg}$, T_{r_avg}, T_{c_avg}-average of synchronous, reluctance and cogging torque
*A-Modulated MMF of armature winding, F_{sa}
†F-Modulated MMF of field winding, F_{sf}
-Dominant components

TABLE IV
MAGNETIC GEAR PAIRS OF TORQUE RIPPLES FOR 6S/(2, 4, 5, 7, 8)R VFRMS

VFRM	Torque ripple	Permeance	kN_r	Source-harmonic order		N_{ripple}
		Λ_{rk}		P_m	P_n	
6s/2r	T_{s_rip}	Λ_{r2}	4	*A-1	†F-3	3
				A-5	F-9	
				A-7	F-3	
	T_{r_rip}	Λ_{r1}	2	A-5	A-7	
	T_{c_rip}	Λ_{r3}	6	F-3	F-3	
6s/4r	T_{s_rip}	Λ_{r2}	8	A-1	F-9	3
				A-5	F-3	
	T_{r_rip}	Λ_{r1}	4	A-1	A-5	
	T_{c_rip}	Λ_{r3}	12	F-3	F-9	
6s/5r	T_{s_rip}	Λ_{r5}	25	A-10	F-15	6
				A-16	F-9	
	T_{r_rip}	Λ_{r4}	20	A-10	A-10	
	T_{c_rip}	Λ_{r6}	30	F-15	F-15	
6s/7r	T_{s_rip}	Λ_{r5}	35	A-14	F-21	6
				A-20	F-15	
	T_{r_rip}	Λ_{r4}	28	A-14	A-14	
	T_{c_rip}	Λ_{r6}	42	F-21	F-21	
6s/8r	T_{s_rip}	Λ_{r2}	16	A-7	F-9	3
				A-13	F-3	
	T_{r_rip}	Λ_{r1}	8	A-1	A-7	
	T_{c_rip}	Λ_{r3}	24	F-9	F-15	

$^{\Delta}T_{s\_rip}$, T_{r_rip}, T_{c_rip}-Ripple of synchronous, reluctance and cogging torque
*A-Modulated MMF of armature winding, F_{sa}
†F-Modulated MMF of field winding, F_{sf}
-Dominant components

(c) For 6s/|6i±1|r (i=0,1,2,…) VFRMs, their torque ripple generated by synchronous torque, reluctance torque and cogging torque are proportional to the 5th, 4th and 6th rotor radial permeance harmonics, respectively. All these permeance harmonics are relatively small compared with the fundamental one. Hence, the 6s/|6i±1|r VFRMs are expected to have smaller torque ripple than 6s/|6i±2|r VFRMs.

The same analysis can also be performed on all the VFRMs listed in Table II. It is found that only the reluctance torque ripple of 6s/|6i±2|r VFRMs and their multiples is proportional to 1st rotor permeance component. Hence, VFRMs with these stator/rotor pole combinations are expected to have larger torque ripple than other VFRMs, as marked by grey color in Table II.

V. FINITE ELEMENT AND EXPERIMENTAL VERIFICATION

A. FEA Verification

In order to verify the revealed torque characteristics of VFRMs, the average torque and torque ripple of (6, 12, 18, 24)s/(2,4,5…20)r VFRMs are compared in Fig. 5. All the machines are globally optimized by FEA using the global optimization module in ANSYS Maxwell package 18.2 under the same constraint listed in Table V. It can be found that:

(a) 6s/(2, 4, 8, 10, 14, 16, 20)r, 12s/(4, 8, 16, 20)r and 24s/(8, 16)r VFRMs show significantly larger torque ripple than other VFRMs, which confirms the conclusion that 6s/|6i±2|r VFRMs and their multiples have large torque ripple generated by their reluctance torque components.

(b) 6s/(7, 11)r, 12s/(10, 14)r, 18s/(17, 19)r and 24s/20r VFRMs have higher average output torque than their counterparts with the same stator slot number, which reveals the conclusion that the stator slot and rotor pole number should be close to each other to achieve the highest output torque.

(c) The higher the stator slot number is, the smaller the output torque will be. The output torque of 12s-VFRMs is approximately half of that of 6s-VFRMs under the same copper loss and machine frame constraints. This can be explained by comparing the 6s/4r and 12s/8r VFRMs:

In a VFRM, the armature current can be calculated by

$$I_a = \frac{1}{N_s N_c}\sqrt{\frac{P_{cua} A_s}{2\rho_{cu}\left(L_{stk} + L_{end}\right)}} \tag{20}$$

where N_c is the tunes per coil; A_s is the total stator slot area; ρ_{cu} is the resistivity of copper; L_{end} is the end length of windings.

Assuming the copper loss of armature winding P_{cua}, total slot area A_s and turns per coil N_c are kept the same for 6s- and 12s-VFRMs, the armature current is proportional to the reciprocal of stator slot number. This also fits field current, i.e.

$$I_a, I_f \propto \frac{1}{N_s} \tag{21}$$

By substituting (21) into (19), yielding:

$$T_{e\_avg} \propto k_T \frac{N_r}{N_s^2} \tag{22}$$

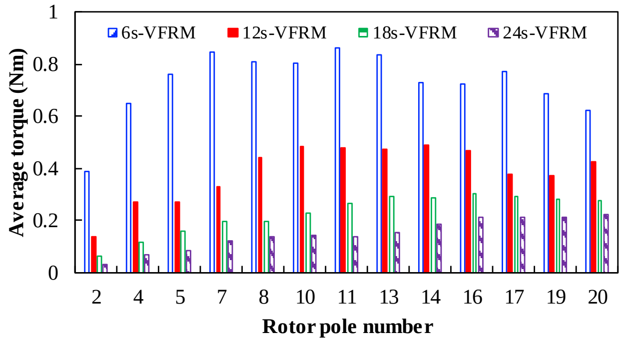

(a)

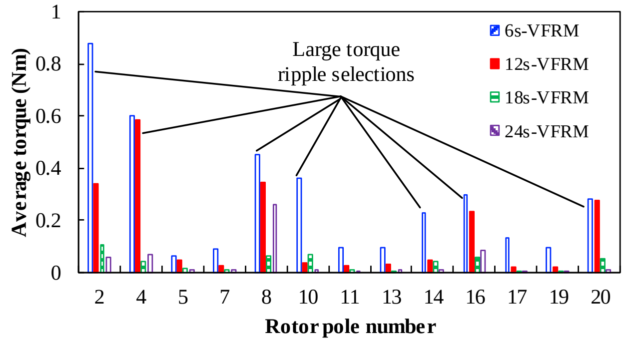

(b)

Fig. 5. Variation of the average torque and torque ripple for (6, 12, 18, 24)s/(2,4,5…20)r VFRMs. (a) Average torque. (b) Torque ripple.

TABLE V
SPECIFICATION CONSTRAINTS FOR GLOBAL OPTIMIZATION

Parameter	Symbol	Unit	Value
Stator outer radius	R_{so}	mm	45
Airgap length	g_0	mm	0.5
Total copper loss	P_{cu}	W	30
Turns per coil (AC/DC)	n_a/n_f	-	183/183
Packing factor	K_f	-	0.5
Stack length	L_{stk}	mm	25

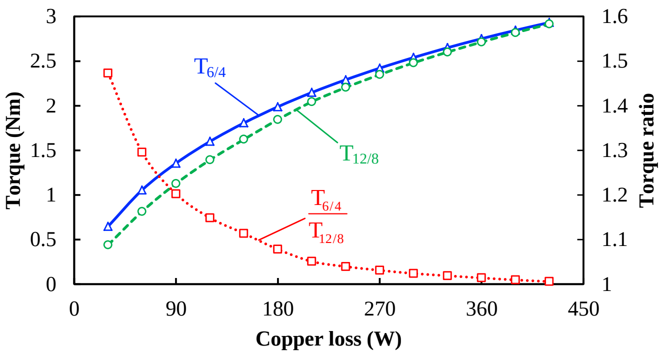

Fig. 6. Variations of torque and torque ratio of 6s/4r and 12s/8r VFRMs optimized under different copper loss constraints.

The 6s/4r and 12s/8r VFRMs are identical in terms of operation principle and torque coefficient k_T. Based on (22), the output torque ratio between these two machines can be obtained, i.e.

$$\frac{T_{6/4}}{T_{12/8}} \propto \frac{4}{6^2} \Big/ \frac{8}{12^2} = 2 \tag{23}$$

It should be noted that the foregoing investigation is based on the assumption that the core saturation is neglected. In this ideal situation, the torque/copper loss ratio of 12s/8r VFRM is proved to be only half of that of 6s/4r VFRM.

However, in a practical situation, two cases should be considered. On one hand, when the copper loss is relatively small and the magnetic saturation level is low, the airgap flux density is mainly determined by the MMF. According to (20)-(23), the amplitude of MMF per coil N_cI is proportional to $1/N_s$, which leads to significantly lower airgap flux density and eventually smaller torque/copper loss ratio in 12s/8r VFRM compared with 6s/4r VFRM. In contrast, when the copper loss is relatively large, the airgap flux density will be limited by the core saturation. In this case, the 6s/4r and 12s/8r VFRMs have similar phase flux linkage and back-EMF, as well as torque/copper loss ratio. This phenomenon is similar to the conclusion in SRMs [20] and can be verified by FEA results of several 12s/8r and 6s/4r VFRMs optimized under different copper loss constraints, as shown in Fig. 6.

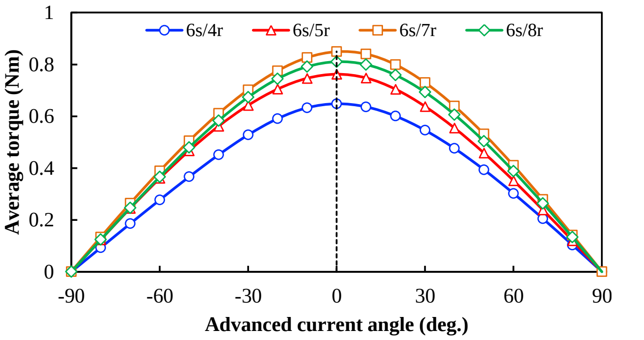

Fig. 7. Variations of average torque with current advanced angle for 6s/(4, 5, 7, 8)r VFRMs (P_{cu}=30W).

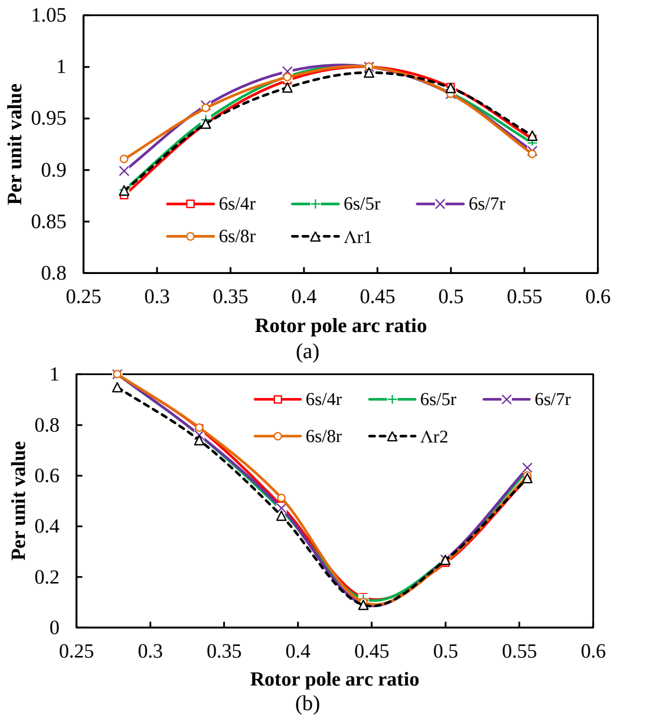

Fig. 8. Variations of per unit value of the average torque, reluctance torque, 1st and 2nd rotor permeance component with rotor pole arc ratio. (a) Average torque and 1st rotor permeance component (b) Reluctance torque and 2nd rotor permeance component.

Considering the fact that 12s/8r VFRM has several advantages over 6s/4r VFRM, i.e., smaller space occupation of slot wedges, smaller slot opening and larger contact area between coil and iron for heat dissipation, 12s/8r VFRM is more suitable for high current density and large frame scale machine design. For low current density and small size machines, a lower slot number is the preferable choice.

Further, it is predicted that the synchronous torque is the dominant part in average torque production since it is proportional to the 1st rotor permeance harmonic. In contrast, the reluctance torque is proportional to the 2nd rotor permeance harmonic and becomes negligible. To verify this, the variations of average torque with the advanced current angle for the optimized 6s/(4, 5, 7, 8)r VFRMs are shown in Fig. 7. The peak values are all obtained when their advanced current angle is close to 0 deg., indicating that the reluctance torque is much smaller than synchronous torque. Then, by using the single-side saliency model developed in [16], the distributions of rotor radial permeance under different rotor pole arc ratio can be obtained from FEA. The average torque and reluctance torque are proved to have similar variation trends with the 1st and 2nd rotor permeance components, as shown in Fig. 8.

B. Experimental Verification

For experimental verification, 6s/7r and 6s/8r VFRMs are prototyped and compared. These two machines share the same stator but different rotors, as shown in Fig. 9. Both the armature and field windings are concentrated types and wound on all the stator teeth. The winding configurations can be found in Fig. 1. The specifications of prototyped machines are listed in Table VI. During the experiments, the field winding is excited by a DC supply while the armature winding is connected to an inverter. The test rig is shown in Fig. 10.

(a)

(b)

Fig. 9. Photos of 6/7 and 6/8 VFRM prototypes. (a) Stator. (b) Rotors.

TABLE VI
MAIN SPECIFICATIONS OF 6/7 AND 6/8 VFRMS

Parameters	Unit	VFRM	
		6/7	6/8
Stator outer diameter	mm	90	
Airgap length	mm	0.5	
Turns per coil (AC/DC)	-	183/183	
Split ratio	-	0.52	
Stator pole arc	deg.	30	
Copper loss	W	30	
Voltage	V	72	
Rated current density	A/mm^2	6	
Rated torque density	Nm/cm^3	5.2	
Rotor pole arc	deg.	23	20

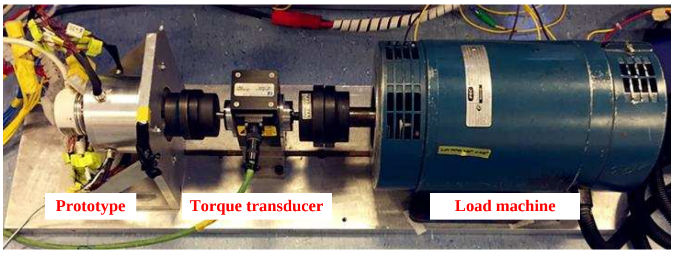

Fig. 10. Test rig.

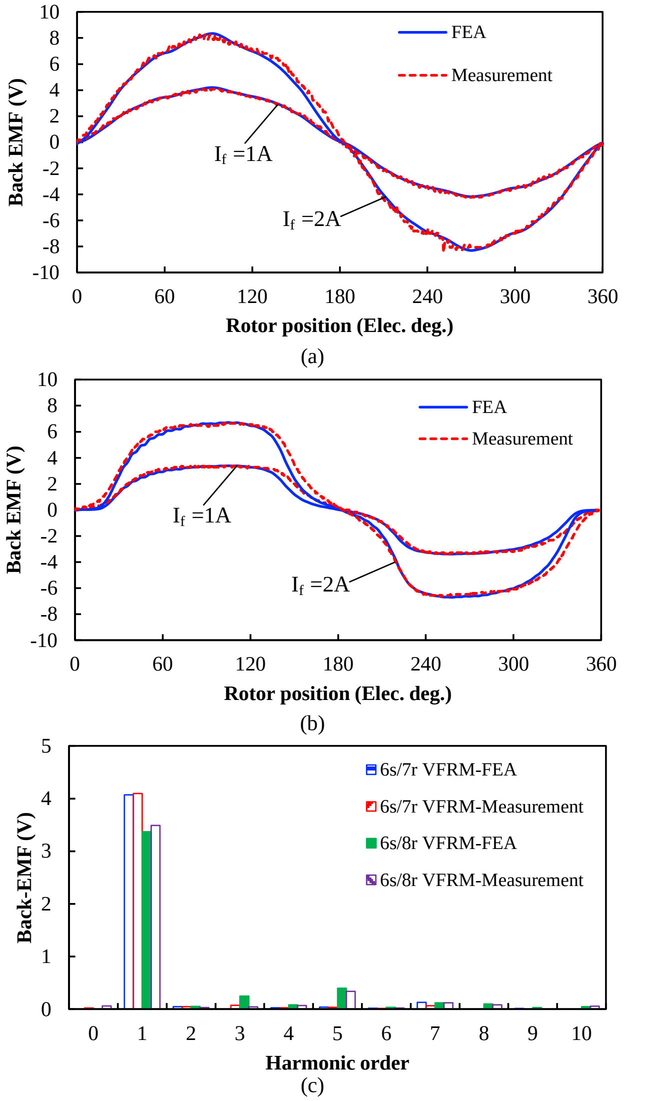

Fig. 11. Back-EMFs of 6/7 and 6/8 VFRMs under 1A and 2A field currents. (a) 6/7 VFRM. (b) 6/8 VFRM. (c) Spectra (I_f=1A).

Firstly, the VFRMs are on open-circuit and only their field windings are excited. The phase back-EMFs are measured, as shown in Fig. 11. Two different field currents are tested and good agreements can be found between FEA and experimental results. From the calculated spectra of back-EMF, it can be seen that the fundamental component of 6s/7r VFRM is significantly larger than 6s/8r VFRM, which indicates the higher output torque of 6s/7r VFRM. Moreover, the back-EMF waveform of 6s/7r VFRM is closer to sinusoidal, whereas the 6s/8r VFRM contains large subharmonics in its back-EMF. Therefore, the 6s/7r VFRM is expected to have smaller torque ripple than 6s/8r VFRM.

Further, the on-load torque characteristics of 6s/7r and 6s/8r VFRMs are measured by torque transducer. The torque waveforms and variations of average torque with RMS currents are shown in Figs. 11 and 12, respectively. It can be seen that the measured torque is slightly smaller than the FEA predicted one. This is mainly due to the measurement error and minor disturbance in the current waveform. Nevertheless, the torque ripple of 6s/8r VFRM is significantly larger than that of 6s/7r VFRM, confirming the prediction in Section IV. Regarding the average torque, the 6s/8r VFRM is smaller than 6s/7r due to its smaller fundamental back-EMF component.

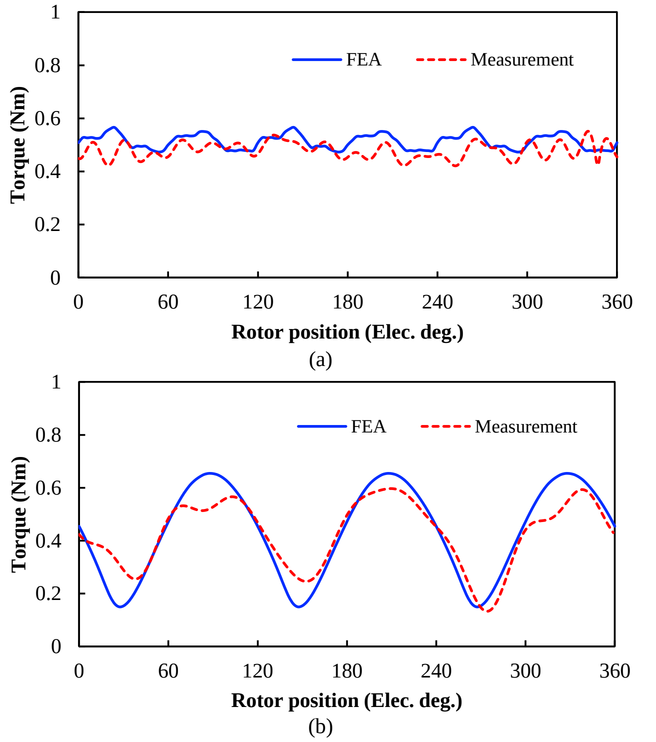

Fig. 12. FEA predicted and measured torque waveforms of 6s/7r and 6s/8r VFRMs when (I_a=I_f=2A). (a) 6s/7r VFRM. (b) 6s/8r VFRM.

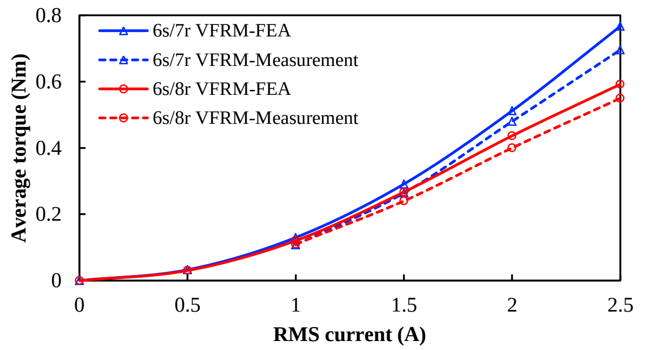

Fig. 13. Variations of average torque with AC RMS current of 6s/7r and 6s/8r VFRMs when (I_a=I_f).

VI. CONCLUSION

In this paper, the stator/rotor pole combinations in VFRMs are investigated based on the magnetic gearing effect. Firstly, the principle of feasible stator/rotor pole selection and corresponding winding configuration is revealed. Then, by identifying the specific magnetic gear pairs which contribute to the synchronous, reluctance and cogging torque components, the torque characteristics in VFRMs are comprehensively illustrated. It is found that:

(a) For all the VFRMs, the synchronous torque is much larger than the reluctance torque in terms of the average torque production. Also, the rotor pole number should be close to the stator slot number to ensure a high output torque.

(b) The 6s/(6i±2)r VFRMs and their multiples exhibit large ripple in their reluctance torque component. Thus, these VFRMs have larger torque ripple than other VFRMs.

(c) VFRMs with a smaller stator slot number are preferable choices to achieve higher torque/copper loss ratio, whereas VFRMs with a higher stator slot number are more suitable for high current density and large frame scale design.

All the analysis and conclusions are validated by FEA on (6, 12)s/(2~20)r VFRMs and by experimental tests on a 6s/7r and 6s/8r VFRM prototypes.

It should be noted that this paper investigates influence of stator/rotor pole combination on torque aspect only. For practical machine design, more aspects including efficiency, power factor, current profile, torque ripple reduction and vibration need to be account for. For example, the power factor will decrease with the increase of rotor pole number under a fixed stator slot number. All these works will be covered in our future work.

REFERENCES

[1] T. Fukami, Y. Matsuura, K. Shima, M. Momiyama, and M. Kawamura, "Development of a low-speed multi-pole synchronous machine with a field winding on the stator side," in Proc. Int. Conf. Elect. Mach., Rome, Italy, 2010, pp. 1–6.

[2] X. Liu, Z. Q. Zhu and Z. P. Pan, "Analysis of electromagnetic torque in sinusoidal excited switched reluctance machines having DC bias in excitation," in Proc. Int. Conf. Elect. Mach., Sept. 2012, pp. 2882-2888.

[3] X. Liu, Z. Q. Zhu, M. Hasegawa, A, Pride, and R. Deodhar, "Vibration and noise in novel variable flux reluctance machine with DC-field coil in stator," in Proc. Int. Conf. Power Electron. Motion Control, Jun. 2012, pp.1100-1107.

[4] X. Liu and Z. Q. Zhu, "Electromagnetic performance of novel variable flux reluctance machines with DC-field coil in stator," IEEE Trans. Magn., vol. 49, no. 6, pp. 3020-3028, Aug. 2012.

[5] X. Liu and Z. Q. Zhu, "Stator/rotor pole combinations and winding configurations of variable flux reluctance machines," IEEE Trans. Ind. Appl., vol. 50, no. 6, pp. 3675–3684, Nov. 2014.

[6] M. Sanada, S. Morimoto, Y. Takeda, and N. Matsui, "Novel rotor pole design of switched reluctance motors to reduce the acoustic noise," in Conf. Rec. IEEE Industrial Applications Conf., Oct. 2000, pp. 107–113.

[7] P. C. Desai, M. Krishnamurthy, N. Schofield, and A. Emadi, "Novel switched reluctance machine configuration with higher number of rotor poles than stator poles: Concept to implementation," IEEE Trans. Ind. Electron., vol. 57, no. 2, pp. 649–659, Feb. 2010.

[8] C. Zhao, H. Qin, and Y. Yan, "Analysis of the pole numbers on flux and power density of IPM synchronous machine," in Proc. PEDS, 2005, vol. 2, pp. 1402–1407.

[9] Z. Q. Zhu, L. J. Wu, and M. L. Mohd Jamil, "Influence of pole and slot number combinations on cogging torque in permanent-magnet machines with static and rotating eccentricities," IEEE Trans. Ind. Appl., vol. 50, no. 5, pp. 3265–3277, Sep./Oct. 2014.

[10] J. T. Chen, Z. Q. Zhu, S. Iwasaki, and R. P. Deodhar, "Influence of slot opening on optimal stator and rotor pole combination and electromagnetic performance of switched-flux PM brushless AC machines," IEEE Trans. Ind. Appl., vol. 47, no. 4, pp. 1681–1691, Jul./Aug. 2011.

[11] K. Wang, Z. Zhu, G. Ombach, M. Koch, S. Zhang, and J. Xu, "Optimal slot/pole and flux-barrier layer number combinations for synchronous reluctance machines," in Proc. 8th Int. Conf. Exhibit. Ecol. Veh. Renew. Energies (EVER), Mar. 2013, pp. 1–8.

[12] X. Liu and Z. Q. Zhu, "Winding Configurations and Performance Investigations of 12-Stator Pole Variable Flux Reluctance Machines," in Proc. of ECCE 2013 Conference, Sep. 15-19, 2013, pp. 1834-1841.

[13] S. Jia, R. Qu, J. Li, D. Li, and R. Zhang, "Stator/rotor slot and winding pole pair combinations of DC biased sinusoidal vernier reluctance machines," in Int. Conf. on Electrical Machine (ICEM), 2016, pp. 904-910.

[14] L.R. Huang, Z.Q. Zhu, J.H. Feng, S.Y. Guo, J.X. Shi, and W.Q. Chu, "Analysis of stator/rotor pole combinations in variable flux reluctance machines using magnetic gearing effect", in IEEE Energy Conversion Congress and Exposition (ECCE2017), pp. 3187-3194, Oct. 2017.

[15] Z. Z. Wu and Z. Q. Zhu, "Analysis of air-gap field modulation and magnetic gearing effects in switched flux permanent magnet machines," IEEE Trans. Magn., vol. 51, no. 5, pp. 1–12, May 2015.

[16] L.R. Huang, J.H. Feng, S.Y. Guo, J.X. Shi, W.Q. Chu, and Z.Q. Zhu, "Analysis of torque production in variable flux reluctance machine," IEEE Trans. Energy Convers., vol. 32, no.4, pp. 1297-1308, Apr. 2017.

[17] B. Hannon, P. Sergeant, and L. Dupré, "Time- and Spatial-Harmonic Content in Synchronous Electrical Machines," IEEE Trans. Magn., vol. 53, no. 3, pp. 1-11, Dec. 2017.

[18] K. Atallah and D. Howe, "A novel high-performance magnetic gear," IEEE Trans. Magn., vol. 37, no. 4, pp. 2844–2846, Jul. 2001.

[19] Ming Chen, Peng Han and Wei Hua, "General airgap field modulation theory for electrical machines," IEEE Trans. Ind. Elec., vol. 64, no. 8, pp. 6063–6074, Aug. 2017.

[20] H. C. Lovatt and J. M. Stephenson, "Influence of the number of poles per phase in switched reluctance motors," Proc. Inst. Elect. Eng., pt. B, vol. 139, no. 4, pp. 307–314, July 1992.

L.R. Huang received the B.Eng. and M.Sc. degrees in electrical engineering from Zhejiang University, Hangzhou, China, in 2012 and 2015, respectively. Since 2015, he has been working toward the Ph.D. degree in the Department of Electronic and Electrical Engineering, University of Sheffield, U.K.
His major research interests include design and application of reluctance machines and permanent magnet machines.

Z.Q. Zhu (M'90–SM'00–F'09) received the B.Eng. and M.Sc. degrees in electrical and electronic engineering from Zhejiang University, Hangzhou, China, in 1982 and 1984, respectively, and the Ph.D. degree in electrical and electronic engineering from The University of Sheffield, Sheffield, U.K., in 1991.
Since 1988, he has been with The University of Sheffield, where he is currently a Professor with the Department of Electronic and Electrical Engineering, Head of the Electrical Machines and Drives Research Group, Royal Academy of Engineering/Siemens Research Chair, Academic Director of Sheffield Siemens Wind Power Research Centre, Director of Sheffield CRRC Electric Drives Technology Research Centre. His current major research interests include the design and control of permanent-magnet brushless machines and drives for applications ranging from automotive to renewable energy.

J.H. Feng (S'06) received his B.S. and M.S. degrees in Electrical Machinery Control from Zhejiang University, China in 1986 and 1989, respectively, and Ph. D. degree in Control Theory and Control Engineering from Central South University, China in 2008. Since 1989, he has been with CRRC Zhuzhou Institute Co. Ltd., Zhuzhou, China, where he is presently the Vice President and Chief Technology Officer. He has published a number of journal and conference proceedings papers. His research interests are modeling, control, and communication of electrical systems, rail networks and high-speed trains. He is also a Guest Professor in Southwest Jiaotong University, Tongji University and Central South University.

S.Y. Guo is a professorial senior engineer. She got graduated from Central South University in December 1981, and serves as the chief technical expert in CRRC Zhuzhou Institute Co., Ltd. in the field of R&D of the electric machine systems for railway locomotive and electrical vehicle applications.

J.X. Shi received the B. Eng. and M. Sc. degrees in electrical engineering from South China University of Technology, Guangzhou, China in 2010 and 2013, respectively. Since 2013, he has been with CRRC Zhuzhou Institute Co., Ltd.
His major research interests include design and application of permanent magnet machines for electrical vehicle applications.

W.Q. Chu (SM'16) received the B. Eng. and M. Sc. degrees in electrical engineering from Zhejiang University, Hangzhou, China in 2004 and Huazhong University of Science and Technology, Wuhan, China in 2007, respectively, and the Ph.D. degree in the electronic and electrical engineering from The University of Sheffield, UK, in 2013.
From 2007 to 2009, he was with Delta Electronics (Shanghai) Co. Ltd. From 2012 to 2014, he was a postdoctoral research associate with The University of Sheffield. Currently, he is a principal design engineer with CRRC Zhuzhou Institute Co. Ltd. His major research interests include the design and analysis of novel machines for wind power and electrical vehicle applications.